

## Supporting Information

### Long-armed hexapod nanocrystals of cesium lead bromide

Shangkun Li, Julie Probst, Philip D. Howes and Andrew J. deMello

Institute for Chemical and Bioengineering, Department of Chemistry and Applied Biosciences, ETH  
Zürich, Vladimir Prelog Weg 1, 8093 Zürich, Switzerland.

#### Experimental Details

##### Materials

Cesium carbonate ( $\text{Cs}_2\text{CO}_3$ , Aldrich, 99.9%), lead bromide ( $\text{PbBr}_2$ , ABCR, 98%), 1-octadecene (ODE, Sigma-Aldrich, 90%), oleylamine (OLA, Acros,  $\geq 96\%$ ), and octanoic acid (Sigma-Aldrich,  $\geq 99\%$ ) were used as received.

##### Preparation of precursor solutions

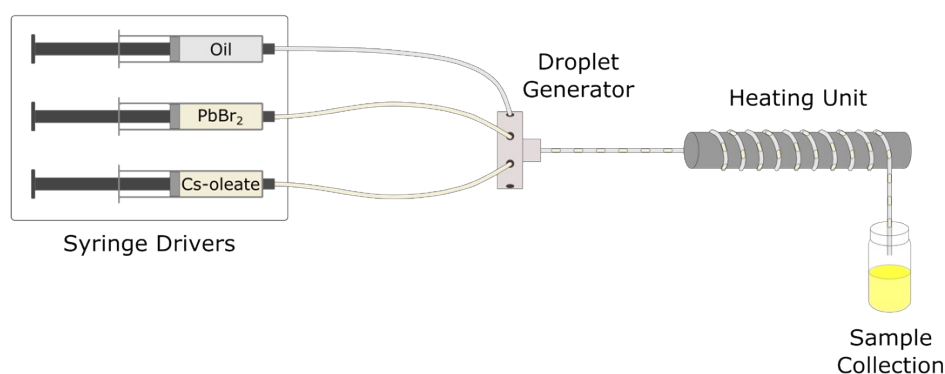
Cesium precursor:  $\text{Cs}_2\text{CO}_3$  (0.156 mmol) was loaded into a 20 mL Schlenk flask together with 10 mL of ODE and 0.8 mL of octanoic acid, dried for 1 h at 120 °C, and then cooled to room temperature under  $\text{N}_2$  before being loaded into a 10 mL Hamilton glass syringe.

Lead bromide precursor:  $\text{PbBr}_2$  (0.188 mmol) was loaded into a 20 mL Schlenk flask along with 5.25 mL of ODE. The cloudy mixture was heated to 120 °C under vacuum, and then 0.25 mL octanoic acid and 1 mL oleylamine were added under  $\text{N}_2$  atmosphere. After the  $\text{PbBr}_2$  dissolved completely, the solution was cooled to room temperature under  $\text{N}_2$  before being loaded into a 10 mL Hamilton glass syringe.

##### Microfluidic synthesis of cesium lead bromide nanosheets

Syringes (10 mL) loaded with precursors were mounted on precision syringe pumps (neMESYS, Cetoni GmbH, Germany). Typically, two syringes were filled with  $\text{PbBr}_2$  precursor and Cs precursor, respectively, while another syringe was used to inject the carrier fluid

(Galden fluorinated fluid, Blaser Swissslube AG, Germany). Precursors and oil were mixed and segmented into droplets at a polyether ether ketone (PEEK) 7-port manifold (0.5 mm thru-hole, IDEX Health & Science, USA). Such a geometry allows precise control of the ratio of carrier phase to dispersed phase. In the final reaction, the volumetric ratio of oil to precursor solution was 1:1, and the molar ratio of Pb to Cs was 1.2:1. Formed droplets subsequently travel through a heating module, where the PTFE tubing is wrapped around a heated copper rod, at 180 °C for 30 s to trigger the reaction.



*Schematic S1. Schematic of the droplet-based microfluidic setup for CsPbBr<sub>3</sub> nanosheet synthesis.*

### **Time-dependent growth of Cs<sub>4</sub>PbBr<sub>6</sub> hexapods**

The reactor was run for 100 minutes, with the crude reaction solution being collected and separated from the carrier fluid. The solution containing CsPbBr<sub>3</sub> nanosheets was stirred at room temperature for up to 36 hours.

### **Growth mechanism study**

The crude reaction solution was collected and divided into 4 vials (1.7 mL in each). Then 0.1 mL octanoic acid, 0.2 mL OLA, 0.5 mL Cs precursor and 1.2 mL PbBr<sub>2</sub> precursor were separately added each. After stirring for 36 hours, TEM samples were prepared with the reaction solution without further purification.

### **Characterization**

TEM was performed on a HT7700 Hitachi TEM at an accelerating voltage of 100 kV. HRTEM was carried on FEI Tecnai F30 FEG at an accelerating voltage of 300 kV. SEM was performed on a Zeiss ULTRA 55. STEM-EDS element spectra and mapping was measured using an FEI Talos F200X at an accelerating voltage of 200 kV. STEM was carried on an FEI Tecnai F30 FEG

at an accelerating voltage of 300 kV. XRD measurements were performed on a PANalytical Empyrean diffractometer equipped with a Cu K $\alpha$  X-ray tube (45 kV, 40 mA). Absorption and photoluminescence spectra were acquired using a custom-built setup, consisting of a broadband light source HL-2000-FHSA (Ocean Optics, Amersham, United Kingdom) for absorption, an LED light source M365LP1 (Thorlabs, Munich, Germany) with 365 nm wavelength as an excitation source for PL, and a fiber-coupled spectrometer USB2000+ (Ocean Optics, Amersham, United Kingdom) for signal detection. Photoluminescence decays were measured on a custom confocal time-correlated single photon counting (TCSPC) set-up. Excitation from a 405 nm picosecond-pulsed diode laser QuixX® 405-120 PS (Omicron, Rodgau, Germany) was coupled by a fiber delivery system and focused on the sample through a 40x magnification microscope objective 40x CFI S Plan Fluor ELWD ADM 40XC, 0.60 NA (Nikon, Zürich, Switzerland). Photoluminescence from the sample was collected through the same objective and reflected by a dichroic mirror Laser Beamsplitter HC BS R405 (Semrock, Rochester, USA). Residual excitation light was filtered by an appropriate long-pass filter 405 LP Edge Basic Longpass Filter (Semrock, Rochester, USA) and reflected by a mirror to the detection path. Photoluminescence light was then focused onto a 30  $\mu$ m pinhole P30S Mounted Precision Pinhole (Thorlabs, Munich, Germany) to reject out-of-focus light, and focused onto a single photon detecting avalanche photodiode MPD PDM Series 50  $\mu$ m (Micro Photon Devices, Bolzano, Italy). The TCSPC electronics are based on the TimeHarp 260 stand-alone module (PicoQuant GmbH, Berlin, Germany).

### **Crystal model of CsPbBr<sub>3</sub> and Cs<sub>4</sub>PbBr<sub>6</sub>**

According to the XRD results, the CsPbBr<sub>3</sub> lattice is the orthorhombic phase (Pnam) and Cs<sub>4</sub>PbBr<sub>6</sub> shows the hexagonal phase (R3c). All crystal models are based on the experimental lattice parameters of CsPbBr<sub>3</sub> ( $a = 8.24$  Å,  $b = 11.74$  Å, and  $c = 8.20$  Å)<sup>1</sup> and Cs<sub>4</sub>PbBr<sub>6</sub> ( $a = b = 13.73$  Å and  $c = 17.30$  Å).<sup>2</sup>

### **FFT pattern analysis**

FFT patterns from four different areas were used to determine the crystal faces. As the FFT patterns were obtained from the HRTEM image via fast Fourier transform, the reciprocating space ruler of the image is 1/nm. Therefore, the lattice distance  $d$  can be calculated by reciprocal of the length  $L$  from diffraction point to centre spot. Then comparing with the PDF card, we can find the similar value of the distance and it corresponds to a specific crystal face.

Two diffraction points (not in the same line crossing the centre spot) were used to determine the crystal faces  $h_1k_1l_1$  and  $h_2k_2l_2$  with the d-spacing of  $d_1$  and  $d_2$ . According to the equation S1, we can get the angle ( $\phi$ ) of these two crystal faces

$$\cos\phi = \frac{h_1h_2 + k_1k_2 + \frac{1}{2}(h_1k_2 + h_2k_1) + \frac{3a^2}{4c^2}l_1l_2}{\sqrt{(h_1^2 + k_1^2 + h_1k_1 + \frac{3a^2}{4c^2}l_1^2)(h_2^2 + k_2^2 + h_2k_2 + \frac{3a^2}{4c^2}l_2^2)}} \quad \text{Equation S1}$$

Then, we can confirm the diffraction point by the angle of two crystal faces. Taking **Figure 2d** as an example, two crystal faces were determined by the value of d-spacing,  $h_1k_1l_1$  (110) and  $h_2k_2l_2$  (300). The angle of these two faces is 30 degrees, which agrees with the result measured from the FFT pattern.

Four zones from the arms and core were selected for high-resolution transmission electron microscopy (HRTEM) examination (**Figure 2a–e** in the main text). FFTs revealed the lattice spacing and crystalline structures (**Figure 2b–e**). In zone 1 from arm I, the observed planes with d-spacing of 0.71 nm (**Figure 2f**) corresponded to the (012) planes of  $\text{Cs}_4\text{PbBr}_6$ .<sup>3</sup> Zones 2 and 3, which were within the core (**Figure 2g and h**), showed lattice fringes of 0.69 nm and 0.40 nm and could be indexed to the (110) and (300) planes of  $\text{Cs}_4\text{PbBr}_6$ . The strong signal from the (110) plane (**Figure 2c and d**) implied that the core was facing towards us in the [001] direction. In zone 4, d-spacings of 0.32 nm and 0.44 nm (**Figure 2i**) were indexed to the (-3-11) and (113) planes of  $\text{Cs}_4\text{PbBr}_6$ , as seen in the FFT (**Figure 2e**).

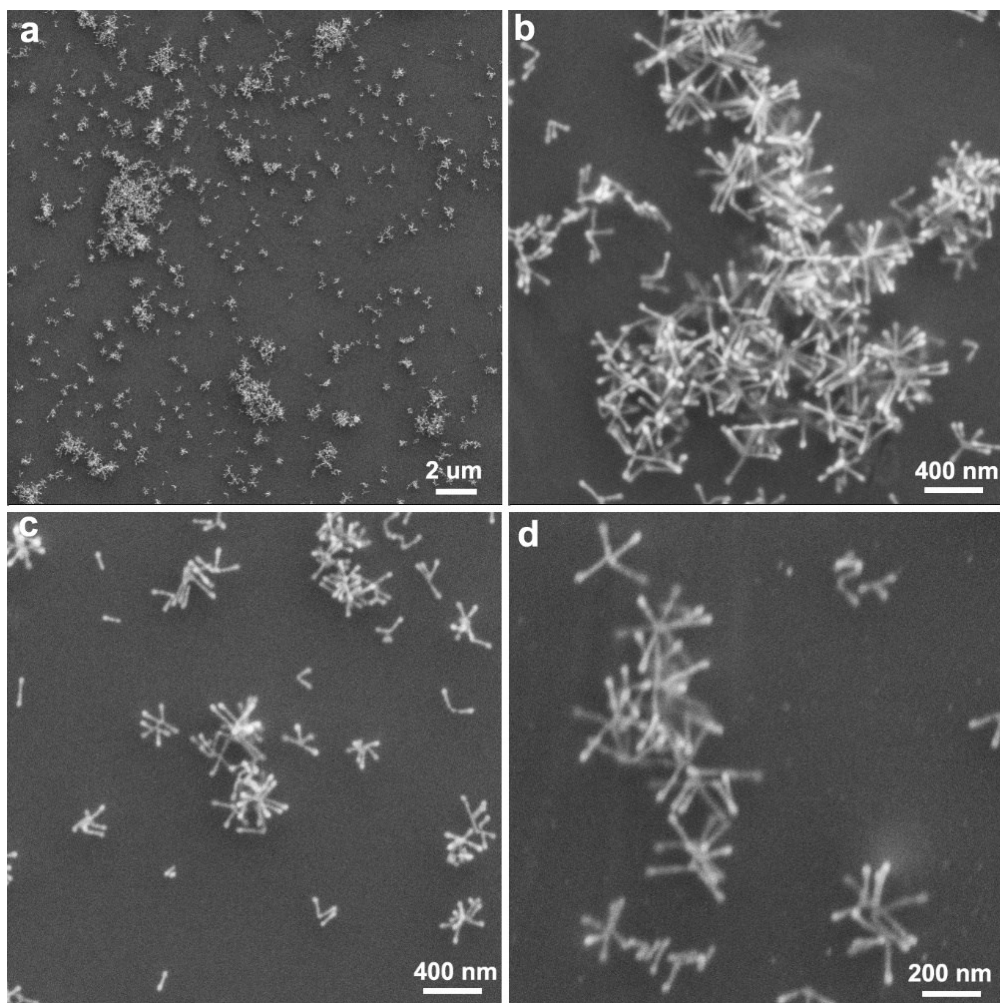
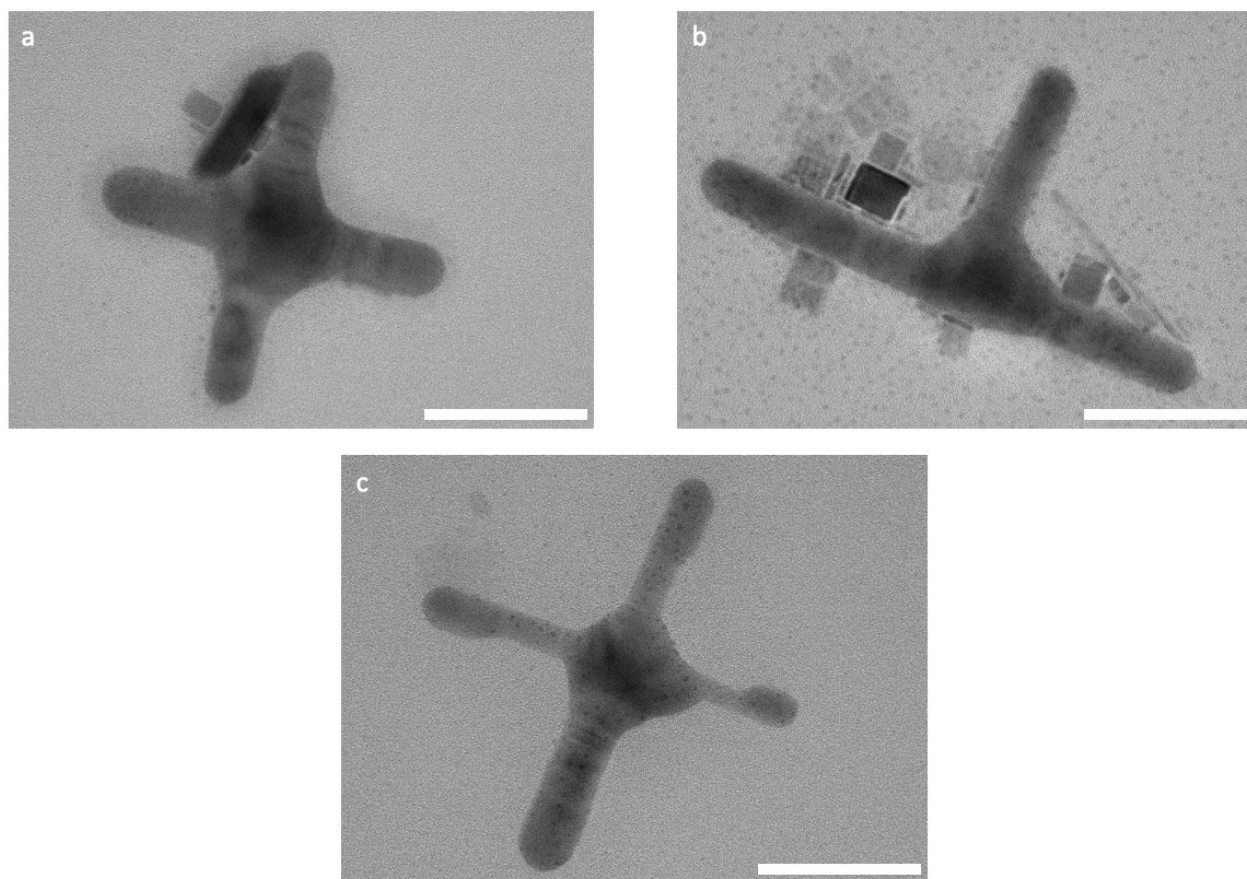
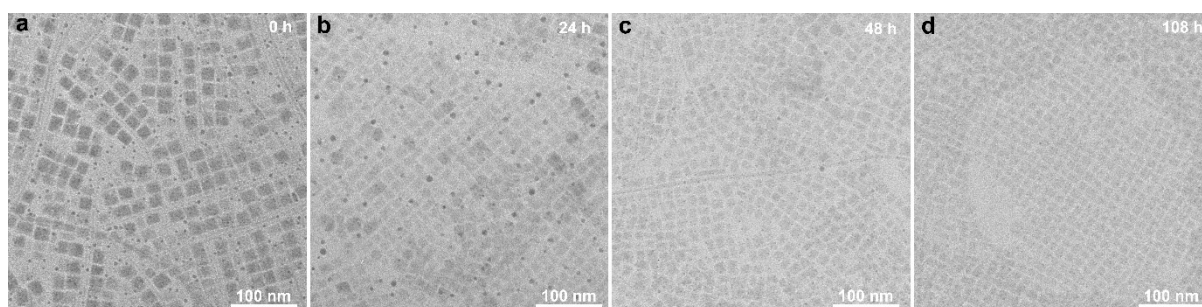


Figure S1. SEM images of the multipods.



*Figure S2. TEM images of multipod structures presenting 90° angles between arms, synthesised under the standard hexapod reaction condition. Scale bar 100 nm.*



*Figure S3. The TEM images of nanosheets dispersing in toluene after purification for 0 h (a), 24 h (b), 48 h (c), and 108 h (d).*

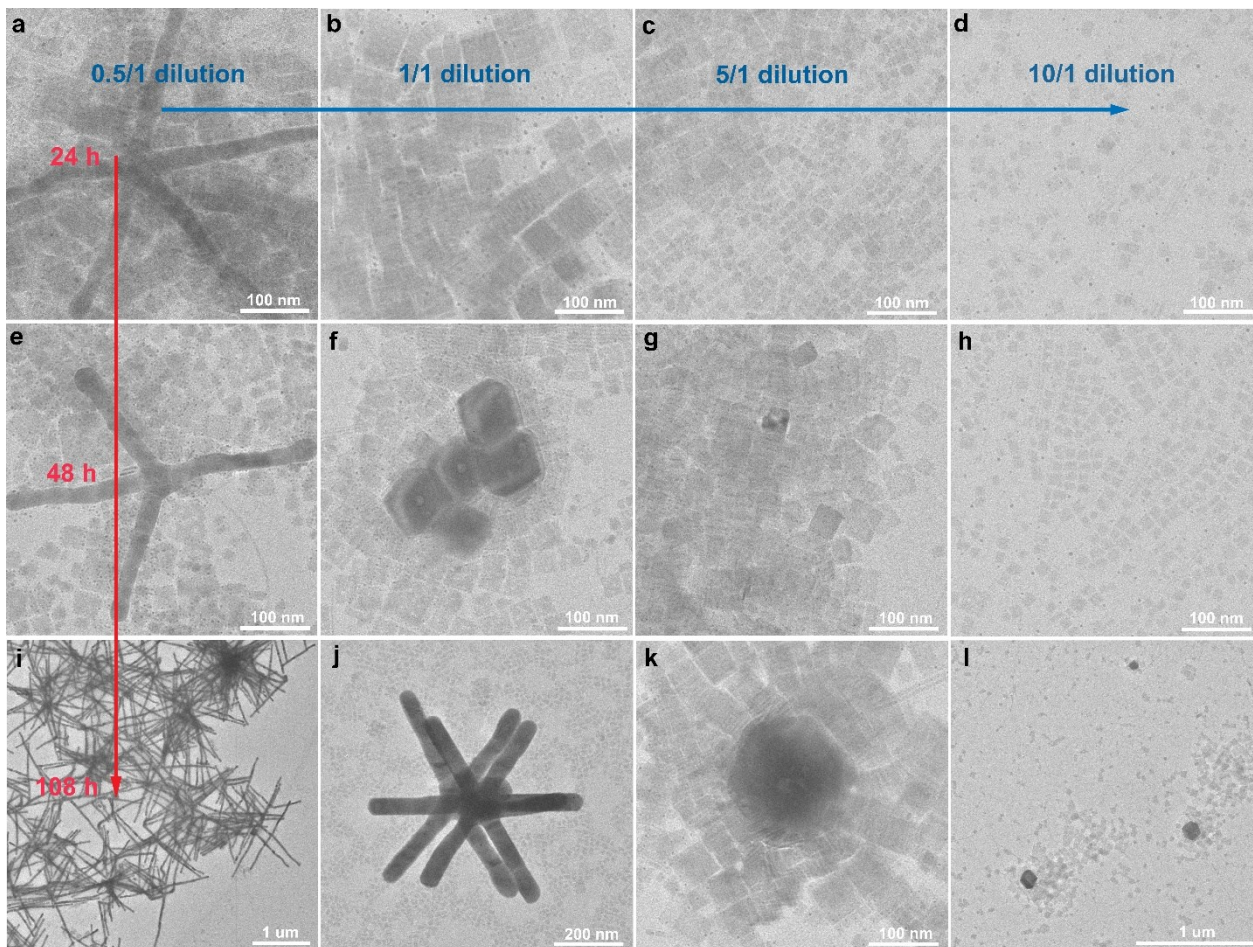


Figure S4. TEM images products formed after different degrees of dilution (in columns labelled in blue). (a-d) after 24 h incubation; (e-h) after 48 h incubation; (i-l) after 108 h incubation.

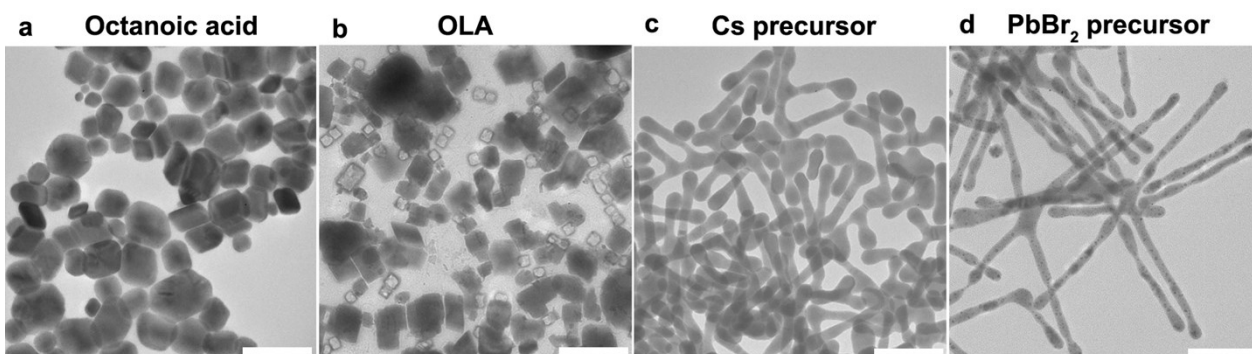


Figure S5. TEM images of the products obtained after different reaction components were added into crude CsPbBr<sub>3</sub> nanosheets solution and stirred for 36 hours. All scale bars are 200 nm.

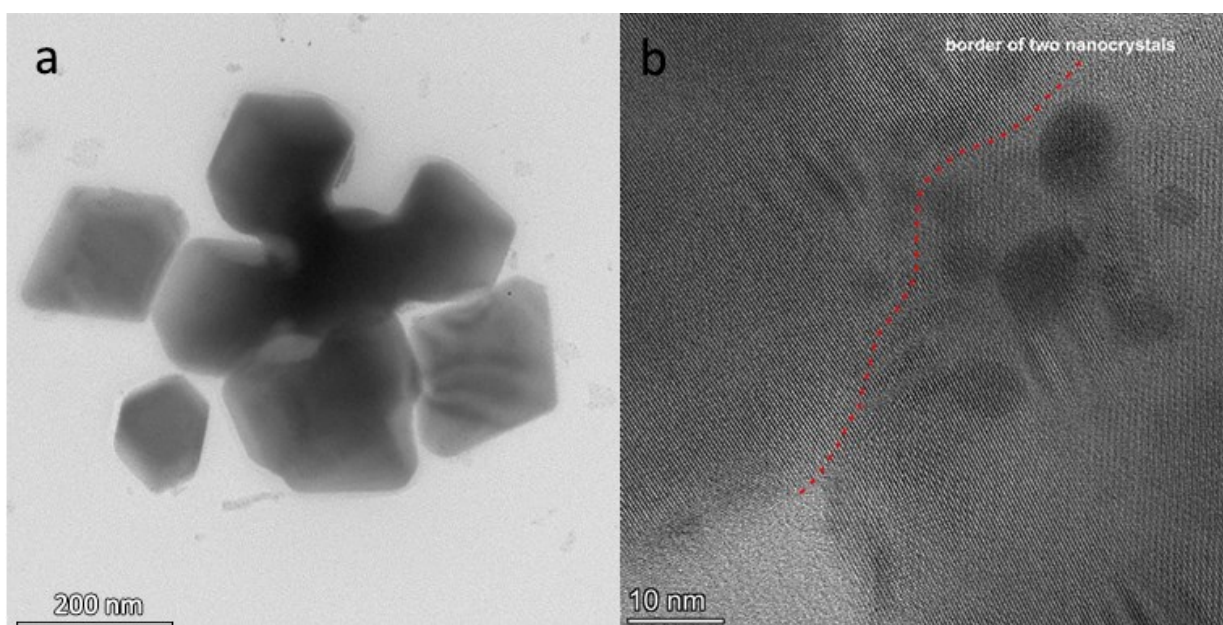


Figure S6. HRTEM images of a) early multipod formation by oriented attachment of rhombic nanocrystal components, and b) two nanocrystals coalescing together under complete crystallographic alignment.

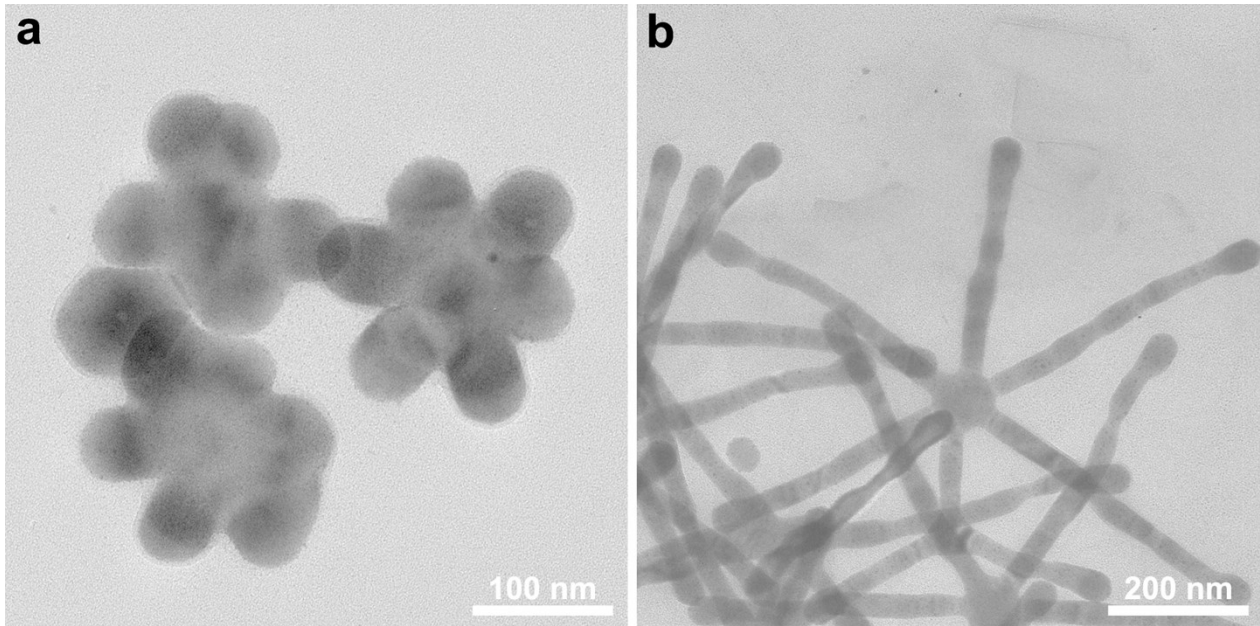


Figure S7. TEM images of hexapod-branched perovskite NCs with different arm lengths. (a) Synthesized without stirring. (b) Synthesized with stirring.

### PL lifetime

To further monitor the emission properties of the evolving species, we performed time-resolved PL measurements by TCSPC measurements. In the current context, evaluation of the PL lifetime increases the contrast of time-integrated PL measurements by revealing whether a change in PL intensity is due to a change in the PL quantum efficiency or to a change in concentration, since the latter does not affect the average lifetime. Evolution of the PL decays over time is shown in Fig. S2a. A triexponential model (black lines) was used to fit the experimental data:

$$y(t) = \sum_{i=1}^n a_i \exp(t/\tau_i) \quad i = 1,2,3 \quad \text{Equation S2}$$

where  $a_i$  is the pre-exponential factor and  $\tau_i$  is the decaytime component. The amplitude-weighted average lifetime can be recovered from the  $a_i$  and  $\tau_i$  values according to the following equation:

$$\tau_{AV \text{ Amp}} = \frac{\sum_{i=1}^n (a_i \tau_i^2)}{\sum_{i=1}^n a_i \tau_i}$$

Equation S3

To obtain adequate fits showing randomly distributed residuals and chi-squared values close to unity, a triexponential model was required, revealing the superposition of fast, medium and slow components.

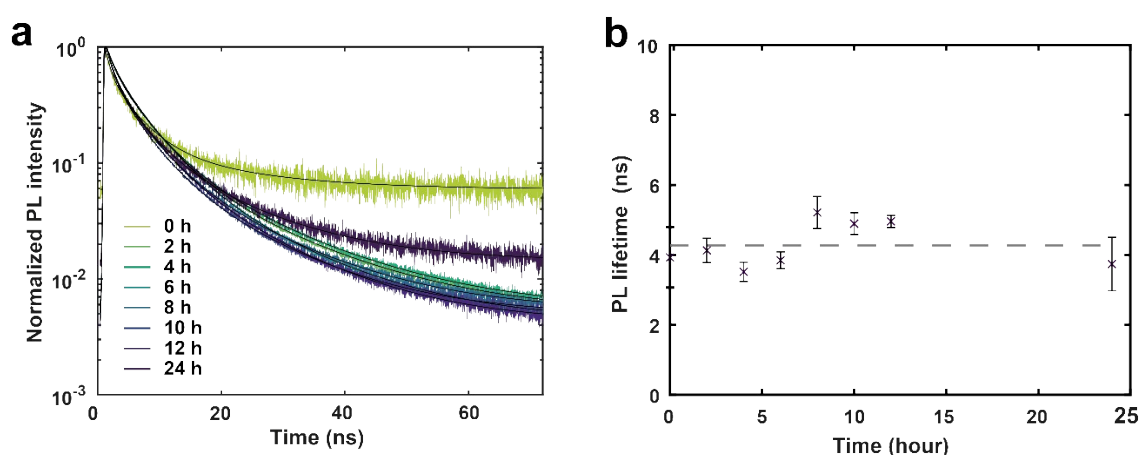


Figure S8. (a) Normalized photoluminescence time-decay (open circles) measured over time with 405 nm excitation. A triexponential decay function was used to fit the data (black lines) and obtain the average lifetime values as shown in (b), where each data point is the average of 5 measurements.

Table S1. Lifetime data at different reaction times. The lifetime components  $\tau_i$  are reported with their corresponding pre-exponential factor  $A_i$ .

time (h)	$\tau_1$ (ns)	$\tau_2$ (ns)	$\tau_3$ (ns)	$A_1$	$A_2$	$A_3$	$\tau_{av}$ (ns)
0	14.60	1.97	3.96	0.10	0.47	0.43	3.93
2	13.90	1.21	4.73	0.10	0.43	0.47	4.13
4	13.40	1.72	3.70	0.08	0.49	0.43	3.52
6	14.22	1.81	3.88	0.09	0.46	0.45	3.85
8	15.78	1.46	5.15	0.12	0.34	0.54	5.21
10	15.80	2.83	3.54	0.12	0.42	0.46	4.89
12	16.00	2.16	4.29	0.11	0.39	0.50	4.96

24	14.40	0.87	3.98	0.12	0.47	0.41	3.74
----	-------	------	------	------	------	------	------

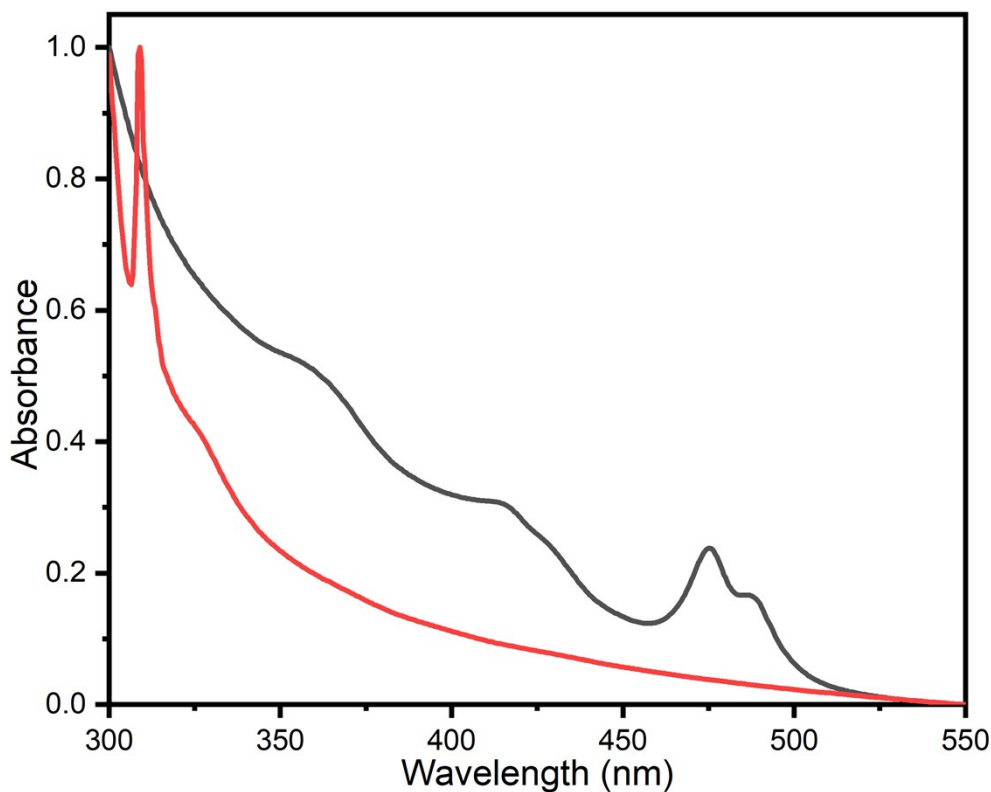


Figure S9. Absorbance spectra of 0 h  $\text{CsPbBr}_3$  nanosheets (black line) and 36 h  $\text{Cs}_4\text{PbBr}_6$  (red line) from deep ultraviolet range.

There is a small blue shift from 313 nm to 309 nm for the absorbance of  $\text{Cs}_4\text{PbBr}_6$ , due to the short ligand used during the synthesis.

### Supporting references

1. Stoumpos, C. C.; Malliakas, C. D.; Peters, J. A.; Liu, Z.; Sebastian, M.; Im, J.; Chasapis, T. C.; Wibowo, A. C.; Chung, D. Y.; Freeman, A. J.; Wessels, B. W.; Kanatzidis, M. G., Crystal Growth of the Perovskite Semiconductor  $\text{CsPbBr}_3$ : A New Material for High-Energy Radiation Detection. *Cryst. Growth Des.* 2013, 13 (7), 2722-2727.
2.  $\text{Cs}_4\text{PbBr}_6$  Crystal Structure: Datasheet from "PAULING FILE Multinaries Edition – 2012" in *SpringerMaterials*. Springer-Verlag Berlin Heidelberg & Material Phases Data System (MPDS), Switzerland & National Institute for Materials Science (NIMS), Japan.

3. Mullin, J. W., *Crystallization*. Elsevier Science: 2001.